A numerical study on the structural integrity of self-anchored cable-stayed suspension bridges

Paolo Lonetti, Arturo Pascuzzo
Department of Civil Engineering, University of Calabria, Via P. Bucci, Cubo39-B, 87030, Rende, Cosenza, Italy
paolo.lonetti@unical.it; 0000-0003-0678-6860
arturo.pascuzzo@unical.it; 0000-0003-3879-6764

ABSTRACT. A generalized numerical model for predicting the structural integrity of self-anchored cable-stayed suspension bridges considering both geometric and material nonlinearities is proposed. The bridge is modeled by means of a 3D finite element approach based on a refined displacement-type finite element approximation, in which geometrical nonlinearities are assumed in all components of the structure. Moreover, nonlinearities produced by inelastic material and second order effects in the displacements are considered for girder and pylon elements, which combine gradual yielding theory with CRC tangent modulus concept. In addition, for the elements of the suspension system, i.e. stays, hangers and main cable, a finite plasticity theory is adopted to fully evaluate both geometric and material nonlinearities. In this framework, the influence of geometric and material nonlinearities on the collapse bridge behavior is investigated, by means of a comparative study, which identifies the effects produced on the ultimate bridge behavior of several sources of bridge nonlinearities involved in the bridge components. Results are developed with the purpose to evaluate numerically the influence of the material and geometric characteristics of self-anchored cable-stayed suspension bridges with respect also to conventional bridge based on cable-stayed or suspension schemes.

KEYWORDS. Self-anchored cable-stayed suspension bridges; Structural integrity; Nonlinear, Plasticity; Ultimate behavior; Finite element method.

OPEN ACCESS

Citation: Lonetti, P., Pascuzzo, A., A numerical study on the structural integrity of self-anchored cable-stayed suspension bridges, Frattura ed Integrità Strutturale, 38 (2016) 358-376.

Received: 01.08.2016
Accepted: 05.09.2016
Published: 01.10.2016

INTRODUCTION

Cable supported bridges are frequently employed to overcome long spans, because of their aesthetic, structural and economic properties, if compared to conventional and standard bridge schemes [1, 2]. However, as the span length increases more advanced analyses are needed to improve safety and reliability of these structures, reproducing accurately all sources of nonlinearities involved in the bridge components. Such task becomes much

important especially for new or advanced bridge configurations such as the ones proposed in the framework of cable-stayed suspension self-anchored schemes, in which, in order to guarantee the reliability of such configurations, it is important to investigate collapse behavior and load carrying capacity of the bridge [3, 4].
In the literature, many research efforts are developed to analyze the influence of geometric and material nonlinearities on the structural behavior of cable supported bridges, especially for cable-stayed configurations. In this framework, the bridge behavior was analyzed by means of two different approaches, which are known as the Bifurcation Point Instability (BPI) and the Limit Point Instability (LPI) approaches. BPI is based on an eigenvalue analysis, which predicts the buckling strength and the corresponding mode shapes of the bridge structure [5-7]. However, since initial imperfections, residual stresses and inelastic behavior of bridge members are not taken into account, this approach may lead to inaccurate results in presence of relevant nonlinearities. As a matter of fact, several studies, based on formulations, which involve both geometric and material nonlinearities, have shown that material inelastic behavior of structural members highly affects the nonlinear static behavior of the bridge structure [8-11]. Both geometric and material nonlinearities were considered in the modified BPI approach proposed by Yoo and Choi [12, 13] in which the effect of material inelasticity in the structural members was reproduced by means of classical tangent modulus theory and column–strength curves provided by current design codes. Moreover, an iterative eigenvalue analysis was adopted to calculate, at each computational step, the tangent modulus of each structural member. However, such approach evaluates only the load-carrying capacity and the corresponding collapse mode, without enter in details in the prediction of the step-by-step behavior or the service bridge configuration. Alternatively, advanced analyses based on step by step integration procedures are proposed in the literature with the purpose to evaluate the complete load-displacement curves. In this framework, the nonlinear inelastic behavior is identified by means of the plastic zone method, which reproduces material nonlinearities arising from the constitutive relationships: globally for the beam-column elements and locally for each fiber of the cross-sections [14-17]. Although plastic zone method leads to accurate results, it requires intensive computational time and cost in the numerical analysis [18]. In addition, the local approach, utilized in material description, introduces mesh dependence effects, which affect the accuracy of the proposed results. In the literature, the load carrying capacity can be also identified by using plastic hinge method, which adopts stability functions and lumped plastic effects at both ends of the elements to capture geometric and material nonlinearities, respectively [19-21]. The considerable advantage of this method is that it is simple in both formulation and implementation and it requires a relatively reduced number of mesh elements in the numerical modeling, avoiding as a result convergence problems and mesh dependence effects of the solution. However, in order to compute accurately the actual response of the structure, the location of the plastic hinges should be known before the analysis. In order to overcome weaknesses of the plastic hinge method and, at the same time, to retain the computational efficiency of the numerical procedure, an hybrid approach based on a fiber hinge beam–column method was developed in [22, 23]. Such method is based on stability functions and fiber model to predict geometric and material nonlinearities, respectively, which are introduced, at discrete number of cross-sections, divided by many fibers, to control the plastic flow in the structure. It is worth noting that the above referred studies, specifically involved in the framework of cable supported bridges, take in account mainly material nonlinearities in both girder and pylons, without introducing any source of nonlinearities in the constitutive elements of the cable system. Such contributions are considered only in rare cases and mainly in the framework of cable-stayed bridges [16, 24]. However, such effects should be taken into account especially in those bridge configurations mostly dominated by the cable system configurations, such as of pure suspension or combined cable-stayed suspension, in which, typically, the cable system plays an important role in the cable force distribution and in the ultimate bridge behavior. Therefore, parametric analyses are quite important especially in the framework of new advanced cable-supported schemes, such as the mixed cable-stayed suspension configurations, whose use, in comparison to existing conventional bridge schemes based on pure cable-stayed or suspension bridges, is quite limited due to the lack investigation and knowledge. This is the case of self-anchored cable-stayed suspension bridges, which especially in the last few years, have received much attention since they are able to combine the best properties of pure cable-stayed and suspension systems leading to structural and economic advantages [25-28]. For this reason, the purpose of present study is to propose an efficient numerical model to analyze the nonlinear static behavior of self-anchored cable-stayed suspension bridges with the purpose to quantify numerically the influence of each source of nonlinearities involved in the bridge components on the ultimate strength of the bridge. To this end, a parametric study in terms of bridge properties, geometric and mechanical characteristics including also comparisons with conventional bridges based on pure cable-stayed and suspension configurations are proposed.
The outline of the paper is as follows: in Section 2 a description of the self-anchored cable-stayed suspension bridge together with the formulation of the bridge modelling and the evaluation of the initial configuration is presented. The numerical implementation is reported in Section 3, whereas in Section 4 numerical comparisons and parametric results in terms of bridge formulations, material properties and geometric characteristics are proposed.

BRIDGE FORMULATION: MAIN EQUATIONS AND INITIAL CONFIGURATION

The structural scheme, reported in Fig. 1, is consistent with a self-anchored cable-stayed suspension bridge, in which the cable system is based on the combination of suspension and cable-stayed configurations. Suspension and cable-stayed cable systems consist of a double layer of cables arranged in the planes containing girder and pylon extremities.

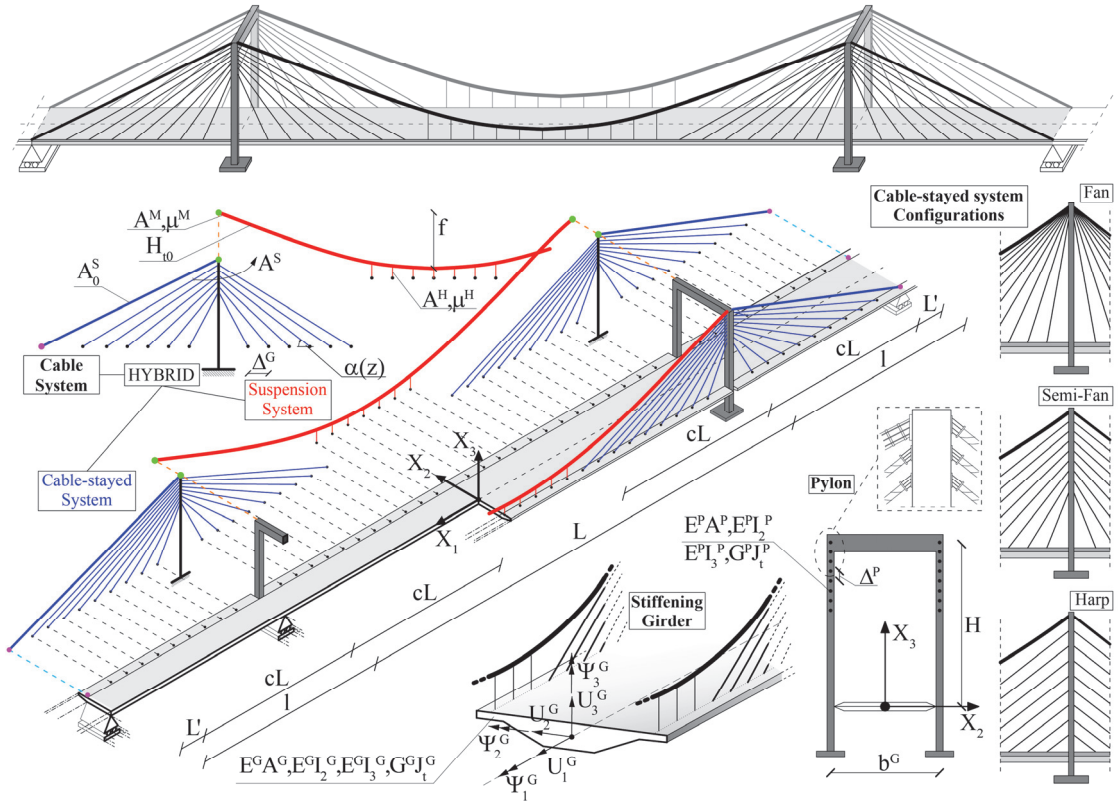

Figure 1: Structural scheme of the self-anchored cable-stayed suspension bridge.

In particular, the cable-stayed system is based on discrete stays, which are mainly arranged in the region close to the pylons, whereas, the suspension system is composed by a main cable and several hangers located in the central part of the main span. The hanger rods and the stays are hinged, at both ends, to the girder and to the main cable or to the girder and pylons and they are spaced at constant step Δ^G along the entire girder length. Furthermore, the stays are spaced at constant step Δ^P along the pylon height and, depending on this step size, the cable-stayed system can be characterized by a fan, a semi-fan or a harp configuration. The main cable is in the central span only and it is hinged at top of the pylons. The cable system is completed by anchor cables, which connect stiffening girder extremities to the top of the pylons. The stiffening girder is simply supported at its ends and at the pylons connections, which are formed by H-shaped configurations.

Initial configuration of the bridge

The initial configuration of the bridge is obtained by using the zero displacement method, which identifies girder and pylon profile under permanent loading by adjusting the initial cable forces to give zero-displacements at the cable anchorages. With reference to the scheme reported in Fig. 2, the unknown quantities are represented by the post-tensioning stresses in the cables (S_i^S, S_i^H, S^M) which are designed by means of the following relationship:

$$\underset{\sim}{S}^C = [S_1^S, \ldots, S_{N^S}^S, S_1^H, \ldots, S_{N^H}^H, S^M] \tag{1}$$

where N^S is the number of stays, N^H is the number of hangers and the superscripts S, H and M refer to the stays (S), hangers (H) and main cable (M), respectively. The displacement conditions utilized to achieve zero displacements at the cable anchorages are expressed as follows:

$$\begin{aligned} &\underset{\sim}{L}^S[(\overline{S}_1^S+\Delta S_1^S,\ldots,\overline{S}_{N^S}^S+\Delta S_{N^S}^S),\underset{\sim}{U}^S]=0\\ &\underset{\sim}{L}^H[(\overline{S}_1^H+\Delta S_1^H,\ldots,\overline{S}_{N^H}^H+\Delta S_{N^H}^H),\underset{\sim}{U}^H]=0\\ &\underset{\sim}{L}^M[(\overline{S}^M+\Delta S^M),U^M]=0 \end{aligned} \tag{2}$$

where $\underset{\sim}{L}^S$, $\underset{\sim}{L}^H$ and $\underset{\sim}{L}^M$ are the constraint operators referred to the stays, hangers and main cable variables, respectively. In Eqs. (2), $\underset{\sim}{U}^S$ is the vector containing horizontal displacements of the left and right top pylon cross-sections, which are identified as $U_1^{P_L}$ and $U_1^{P_R}$, respectively, and vertical displacements of the stays at the girder connections:

$$\left[\underset{\sim}{U}^S\right]^T=[U_1^{P_L},U_1^{P_R},U_{3,S(1)}^G,\ldots,U_{3,S(N^S)}^G] \tag{3}$$

Moreover, $\underset{\sim}{U}^H$ is the vector containing vertical displacements of the hangers at the girder connections, i.e. $\left[\underset{\sim}{U}^H\right]^T=[U_{3,H(1)}^G,\ldots,U_{3,H(N^H)}^G]$. Finally, U^M is the vertical displacement of the main cable at the midspan cross-section. It is worth noting that, in Eqs. (2), the total initial stress is expressed as a combination of a constant quantity $(\overline{S}_i)^{S,H,M}$ and an incremental contribution $(\Delta S_i)^{S,H,M}$. The former is a set of trial initial post-tensioning cable forces, which are estimated by means of simple design rules commonly adopted and verified in the context of long-span bridges [1, 29-32], whereas the latter is defined by an additional stress vector, whose components correspond to unknown quantities to be identified.

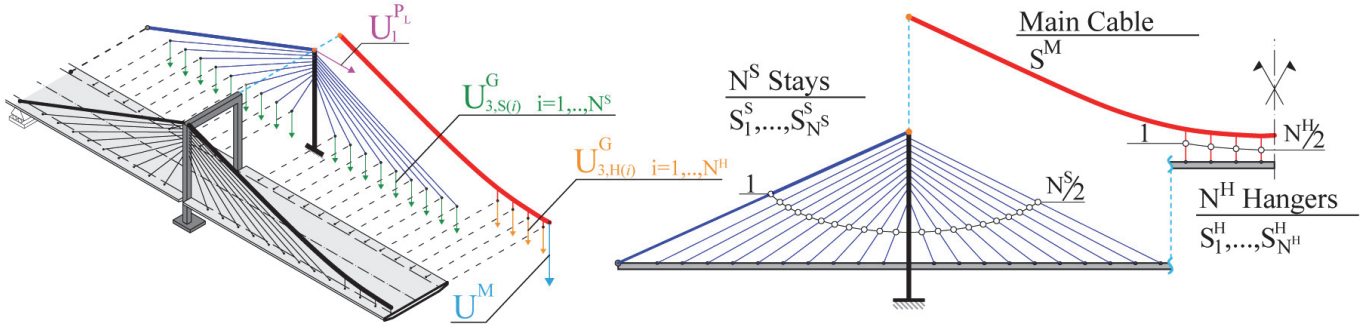

Figure 2: Displacement and control variables for initial configuration.

Girder and pylons

The kinematic model is consistent with a geometric nonlinear Euler-Bernoulli theory, in which moderately large rotations are considered. The torsional behavior owing to eccentric loading is described by means of classical De Saint Venant theory. In addition, since girder and pylons are mainly subjected to axial forces and bending moments, the nonlinear material behavior can be taken into account by a gradual yielding theory based on the combination of the Column Research Council (CRC) tangent modulus concept and a plastic hinge model [33]. The former is suitable to take into account for gradual yielding along the length of an axially loaded element between plastic hinges, whereas the latter is used to represent the partial plasticization effect associated to bending mechanisms. Starting from the status obtained in the initial configuration, in which only dead and permanent loads are considered, the internal stresses are defined by the following relationships between generalized strain and stress variables as follows:

$$
\begin{aligned}
N_1 &= N_1^0 + E_t A\varepsilon_1 = N_1^0 + E_t A\left\{U_{1,X_1} + \frac{1}{2}[U_{1,X_1}^2 + U_{2,X_1}^2 + U_{3,X_1}^2]\right\},\\
M_2 &= M_2^0 + \eta E_t I_2 \chi_2 = M_2^0 + \eta E_t\ I_2 \Psi_{2,X_1} = M_2^0 - \eta E_t I_2 U_{3,X_1 X_1},\\
M_3 &= M_3^0 + \eta E_t I_3 \chi_3 = M_3^0 + \eta E_t\ I_3 \Psi_{3,X_1} = M_3^0 + \eta E_t\ I_3 U_{2,X_1 X_1},\\
M_1 &= GJ_t \Theta\ = GJ_t\ \Psi_{1,X_1}
\end{aligned}
\tag{4}
$$

where E_tA and ε_1 are the axial stiffness and strain, χ_2 and χ_3 or E_tI_2 and E_tI_3 are the curvatures or the bending stiffnesses with respect to the X_2 and X_3 axes, respectively, Θ and GJ_t are the torsional curvature and stiffness, respectively, N_1 is the axial stress resultant, M_2 and M_3 are the bending moments with respect to the X_2 and X_3 axes, respectively, and M_1 is the torsional moment. Moreover, N_1^0, M_2^0 and M_3^0 are the initial axial force and bending moments with respect to the X_2 and X_3 axes, respectively. The CRC tangent modulus can be expressed as [34] (Fig. 3):

$$
\begin{aligned}
E_t &= 1.0E \qquad\qquad \text{for} \quad N_l \le 0.5P_y\\
E_t &= 4\frac{N_1}{P_y}E\left(1-\frac{N_1}{P_y}\right) \qquad \text{for} \quad N_l > 0.5P_y
\end{aligned}
\tag{5}
$$

where E is the elastic modulus of the member, P_y is the plastic axial strength.

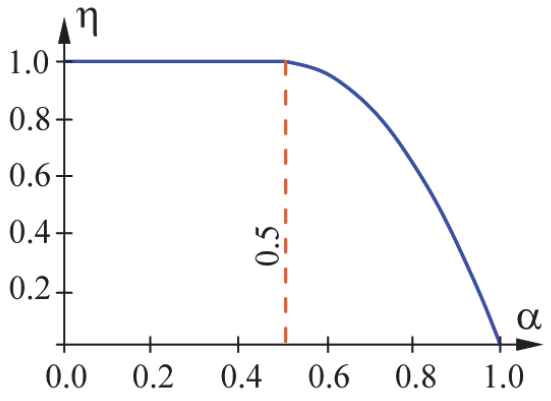

Figure 3: Stiffness reduction for the plastic hinge model.

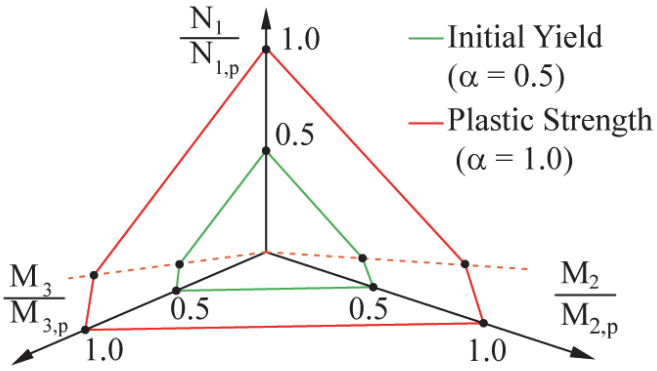

Figure 4: Full plastic surface based on AISC-LRFD.

The gradual inelastic bending stiffness reduction is expressed by a dimensionless reduction parameter η which is assumed to vary according to the following parabolic functions:

$$
\begin{aligned}
\eta &= 1.0 \qquad\qquad \text{for} \quad \alpha \le 0.5\\
\eta &= 4\alpha(1-\alpha) \qquad \text{for} \quad \alpha > 0.5
\end{aligned}
\tag{6}
$$

where α is a force-state parameter which measures the magnitude of axial force and bending moment at the element end. The damage parameter α can be expressed by AISC-LRFD interaction domain (Fig. 4), which defines the cross-section plastic strength of the element as:

$$
\begin{aligned}
\alpha &= \frac{N_1}{P_y} + \frac{8}{9}\frac{M_2}{M_{2,p}} + \frac{8}{9}\frac{M_3}{M_{3,p}} \qquad \text{for} \quad \frac{N_1}{P_y} \ge \frac{2}{9}\frac{M_2}{M_{2,p}} + \frac{2}{9}\frac{M_3}{M_{3,p}}\\
\alpha &= \frac{N_1}{2P_y} + \frac{M_2}{M_{2,p}} + \frac{M_3}{M_{3,p}} \qquad \text{for} \quad \frac{N_1}{P_y} < \frac{2}{9}\frac{M_2}{M_{2,p}} + \frac{2}{9}\frac{M_3}{M_{3,p}}
\end{aligned}
\tag{7}
$$

where $M_{2,p}$ and $M_{3,p}$ are the full plastic moments of the X_2 and X_3 axes, respectively. More details on the definition of Eqs.(6)-(7) can be recovered in [33].

Cable elements

The nonlinear behavior of the cables is defined according to finite deformation theory in which large displacement effects and inelastic behavior due to plastic deformations are considered.

In order to reproduce kinematic nonlinearities arising from the sag effect, a multiple truss element formulation is considered, in which each cable or part of cable is discretized by using multiple truss elements [35-37]. The strain measure is described by Green-Lagrange tensor, which is defined, consistently to Green-Nadghi approach [38, 39]. Therefore, the description of the stress variable coincides with the Second Piola-Kirchhoff stress, which can be expressed as:

$$S_1^C = C\left(E_1^C - E_{1,p}^C\right) + S_0^C \quad \text{with} \quad E_1^C = U_{1,X_1}^C + \frac{1}{2}\left[U_{1,X_1}^2 + U_{2,X_1}^2 + U_{3,X_1}^2\right]^C \tag{8}$$

where E_1^C is the total axial strain, $E_{1,p}^C$ is the axial plastic strain and S_0^C is the initial stress.

A scalar valued variable, i.e. α^C, is considered to describe isotropic hardening evolution law, by means of a classical linear relationship. Moreover, it is postulated the existence of a convex, differentiable yield function expressed in the stress space by means of the following expression:

$$\overline{f} = f(S_1^C, E_{1,p}^C, \alpha^C) = S_1^C - S_{y0}^C - K\alpha^C \tag{9}$$

where S_{y0}^C and K are the initial hardening threshold and the evolution parameter, respectively. Consistently with classical plasticity approach, the evolution of the plastic variables is based on a standard formulation, whose incremental relationship is defined according to the normality evolution rule, i.e. $E_{1,p}^C = \lambda^* \partial\overline{f}/\partial S_1^C$.

Finally loading-unloading relationships concerning the consistency of the incremental constitutive equations can be defined by the following expressions:

$$\lambda^* \geq 0, \overline{f} \leq 0 \quad \text{and} \quad \lambda^* \overline{f} = \lambda^* \dot{\overline{f}} = 0 \tag{10}$$

FINITE ELEMENT IMPLEMENTATION

The governing equations reported in the previous section introduce a nonlinear differential system, whose analytical solution is quite complex to be extracted. As a consequence, a numerical approach based on the finite element formulation is utilized. In particular, the weak forms for the *i*-th finite element related to the girder (*G*), pylon (*P*) and the cable system (*C*), respectively, are defined by the following expressions:

Girder and Pylon

$$\begin{aligned}
&\int_{l_e^i} N_1^{G(P)}\left(1 + U_{1,X_1}^{G(P)}\right) w_{1,X_1} dX_1 - \sum_{j=1}^{2} N_{1j}^{G(P)} U_{1j}^{G(P)} = 0 \\
&\int_{l_e^i} \left\{-M_2^{G(P)} w_{2,X_1X_1} + \left(N_1^{G(P)} U_{3,X_1}^{G(P)}\right) w_{2,X_1}\right\} dX_1 - \sum_{j=1}^{2} T_{3j}^{G(P)} U_{3j}^{G(P)} - \sum_{j=1}^{2} M_{2j}^{G(P)} \Psi_{3j}^{G(P)} = 0 \\
&\int_{l_e^i} \left\{M_3^{G(P)} w_{3,X_1X_1} + \left(N_1^{G(P)} U_{2,X_1}^{G(P)}\right) w_{3,X_1}\right\} dX_1 - \sum_{j=1}^{2} T_{2j}^{G(P)} U_{2j}^{G(P)} - \sum_{j=1}^{2} M_{3j}^{G(P)} \Psi_{2j}^{G(P)} = 0 \\
&\int_{l_e^i} M_1^{G(P)} w_{4,X_1} dX_1 - \sum_{j=1}^{2} M_{1j}^{G(P)} \Psi_{1j}^{G(P)} = 0
\end{aligned} \tag{11}$$

Cable system

$$\begin{aligned}
&\int_{l_e^i} N_1^C \left(1+U_{1,X1}^C\right) w_{1,X_1} dX_1 - \int_{l_e^i} b_1 w_1 dX_1 - \sum_{j=1}^{2} N_{1j} U_{1j}^C = 0 \\
&\int_{l_e^i} N_1^C w_{2,X_1} dX_1 - \sum_{j=1}^{2} T_{2j}^C U_{2j}^C = 0 \\
&\int_{l_e^i} N_1^C w_{3,X_1} dX_1 - \int_{l_e^i} b_3 w_3 dX_1 - \sum_{j=1}^{2} T_{3j}^C U_{3j}^C = 0
\end{aligned} \tag{12}$$

where $(N_{1j}, T_{2j}, T_{3j}, M_{1j}, M_{2j}, M_{3j})^k$ with $k = C,G,P$ represent the internal forces applied at the end nodes of the generic cable, girder or pylon element. Finite element expressions are written starting from the weak forms previously reported, introducing Hermit cubic interpolation functions for the girder and pylon flexures in the X_1X_2 and X_2X_3 deformation planes and Lagrange linear interpolation functions for the cable system variables and the remaining variables of the girder and the pylons:

$$\underset{\sim}{U}^C(\underset{\sim}{r},t) = \underset{\sim}{N}^C(\underset{\sim}{r})\underset{\sim}{q}^C(t), \quad \underset{\sim}{U}^G(\underset{\sim}{r},t) = \underset{\sim}{N}^G\underset{\sim}{q}^G(t), \quad \underset{\sim}{U}^P(\underset{\sim}{r},t) = \underset{\sim}{N}^P\underset{\sim}{q}^P(t) \tag{13}$$

where $\underset{\sim}{q}^C$, $\underset{\sim}{q}^G$, $\underset{\sim}{q}^P$ are the vectors collecting the nodal degrees of freedom of the cable, girder and pylon respectively, $\underset{\sim}{N}^C, \underset{\sim}{N}^G, \underset{\sim}{N}^P$ are the matrixes containing the displacement interpolation functions for cable element (*C*), girder (*G*) and pylons (*P*), $\underset{\sim}{r}$ is the local coordinate vector of the *i*-th finite element. The discrete equations in the local reference system of the *i*-th element are derived substituting Eq. (13) into Eqs. (11)-(12), leading to the following equations in matrix notation:

$$\underset{\sim}{K}^i\underset{\sim}{U}^i = \underset{\sim}{P}^i + \underset{\sim}{R}^i \qquad \text{with } i = G,P,C \tag{14}$$

where $\underset{\sim}{K}^i$ is the stiffness matrix, $\underset{\sim}{P}^i$ is the load vector produced by the dead and live loading, $\underset{\sim}{R}^i$ is the unknown force vector collecting point sources. In order to reproduce the bridge kinematic correctly, additional relationships to define the connections between girder, pylon and cable system should be introduced. In particular, the cable system displacements should be equal to those of the girder and the pylons at the corresponding intersection points. Hence, the bridge kinematic is restricted by means of the following constrain conditions:

$$U_3^G\left(\underset{\sim}{X}_{C_i},t\right) + \Psi_1^G\left(\underset{\sim}{X}_{C_i},t\right)\frac{b^G}{2} = U_3^C\left(\underset{\sim}{X}_{C_i},t\right), \quad U_1^G\left(\underset{\sim}{X}_{C_i},t\right) - \Psi_3^G\left(\underset{\sim}{X}_{C_i},t\right)\frac{b^G}{2} = U_1^C\left(\underset{\sim}{X}_{C_i},t\right) \tag{15}$$

$$U_1^P\left(\underset{\sim}{X}_P,t\right) = U_1^C\left(\underset{\sim}{X}_P,t\right), \quad U_2^P\left(\underset{\sim}{X}_P,t\right) = U_2^C\left(\underset{\sim}{X}_P,t\right), \quad U_3^P\left(\underset{\sim}{X}_P,t\right) = U_3^C\left(\underset{\sim}{X}_P,t\right) \tag{16}$$

where $\underset{\sim}{X}_{C_i}$ and $\underset{\sim}{X}_P$ represent the vectors containing the intersection positions of the *i*-th cable element and the pylon top cross section, respectively, (U_1^G, U_3^G) and (Ψ_1^G, Ψ_3^G) are the displacement and rotation fields of the centroid axis of the girder with respect to the global reference system, respectively. It is worth nothing that, Eqs. (15) are constraint equations imposed between the off-set nodes of the girder and those associated to the cable elements.

Finally, starting from Eqs.(14) taking into account of Eqs. (15)-(16) as well as the balance of secondary variables at the interelement boundaries, the resulting equations of the finite element model are:

$$\underset{\sim}{K}\underset{\sim}{Q} = \underset{\sim}{T} \tag{17}$$

where $\underset{\sim}{Q}$ with $\underset{\sim}{Q} = \underset{\sim}{U}^C \cup \underset{\sim}{U}^G \cup \underset{\sim}{U}^P$ is the generalized coordinate vector containing the kinematic variables associated with the girder, the pylons and the cable system, $\underset{\sim}{K}$ is the global stiffness matrix and $\underset{\sim}{T}$ is the loading vector. Since the structural behavior of each element depends on the deformation state of the members, the governing equations defined by Eq. (17) will change continuously as the structure deforms.

The governing equations are solved numerically, by using a user customized finite element program, i.e. COMSOL Multiphysics [40], which allows to introduce directly weak forms defined by Eqs. (11)-(12) on the basis of the adopted numerical approximation of the kinematic fields, namely Eqs. (13). The resulting equations correspond to the discrete or algebraic nonlinear expressions defined by Eq. (17). It is worth noting that the structural response for each load increment is obtained by means of an iterative and incremental procedure, which considers both geometric and material nonlinearities arising from bridge constituents. For this reason, the finite element model of the structure is coupled with several equation-based models, each of them related to definition of the inelastic properties of cables, pylons and girder. For each load increment, plastic variable rate related to each structural element are determined at each cross-section to calculate the current stiffness of the bridge components. Subsequently, current stiffness matrix as well as load vector are updated on the basis of the values arising from the previous converged step.

RESULTS

In the present study, the bridge dimensioning is selected in accordance with values utilized in practical applications and due to both structural and economic reasons [29, 30, 41]. The bridge configuration is defined by using dimensionless parameters. In particular, values of dimensionless cable-stayed part length $(c = L_{CS}/L)$, height-span ratio $(\mu = H/cL)$ and rise to main span length ratio $(\varsigma = f/L)$, within the following ranges $0.25 \le c \le 0.45$, $0.40 \le \mu \le 0.50$ and $0.05 \le \varsigma \le 0.20$ are considered. The girder cross-section is assumed to be single box section with variable depth (h^G), constant width (b^G) and thickness (δ^G) equal to 33 m and 0.033 m (Tab. 1). The variability of the girder depth is expressed as a function of the bending stiffness ratio, between the girder and the cable system $(\varepsilon_F = \sqrt[4]{4I_2^G\sigma_G/H^3 g})$, which usually takes values between 0.25 and 0.35. The pylon cross-section is also assumed to be single box section with depth (h^P) and width (b^P) expressed as a function of the girder/pylon bending stiffness ratio $(I_r = I_2^P / I_2^G)$, and taken in the range between 1 and 100. Moreover, depth to width ratio (h^P/b^P) and thickness (δ^P) are fixed equal to 1.5 and $(b^P/100)$, respectively. Both girder and pylons are made of steel with elasticity modulus $(E^{G,P})$, yield stress $(S_y^{G,P})$ and specific weight $(\gamma^{G,P})$, equal to 2.1×10^5 MPa, 450 MPa and 78.5 kN/m^3, respectively. Stays and hangers are uniformly distributed along the girder with spacing step (Δ^G) equal to a 20 m. Moreover, four cable-stayed system configurations are considered: fan, harp and two semi-fan layouts. In the latter cases, starting from the top of the pylons, the stays are distributed along the height with a constant step (Δ^P) equal to H/200 or H/500. Cable cross-sections are designed on the basis of practical design rules, typically, accepted in the framework of cable-supported bridges [29], which are expressed by the following equations:

$$A_i^S = \frac{g^G \Delta^G}{S_g^S \sin\alpha_i},\quad A_i^H = \frac{g^G \Delta^G}{S_g^H},\quad A_i^H = \frac{H_{t0}}{S_A \cos\phi} \tag{18}$$

where p is the per unit length live loads, a_i is the angle between stay and girder, ϕ is the orientation angle formed by the main cable tangent at pylon intersection and the horizontal direction, H_{t0} horizontal axial force, which can be expressed as $H_{t0} = [0.25 a_m (g^G + p)(L - 0.5 a_m)]$, with a_m the projection length on the girder of the hanger position (Fig. 1). Moreover, S_g^S and S_g^H represent the initial stress for stays and hangers, respectively, which are expressed by means of the following expression:

$$S_g^{S,H} = \frac{g^G}{g^G + p} S_A^C \tag{19}$$

where S_A^C is the admissible stress of cable elements. The elastic modulus (E^C) and the admissible stress (S_A^C) of cable elements are assumed equal to 2.1×10^5 MPa and 1.6×10^3 MPa, respectively. The girder dead load g^G is defined as $1.4 A^G \gamma^G + 60$ kN/m, where A^G is the girder cross-section and 1.4 is a magnification factor of the dead load to consider diaphragms and other utilities installed in the girder. Moreover, the amount equal to 60 kN/m represents the weight of the other structural and nonstructural elements such as pavement, street lamps, and other attachments [13]. Without loss

of generality, in all analyses only live loads (p) concerning traffic loads are considered, which are combined with dead loads by using unfactored loading combinations.

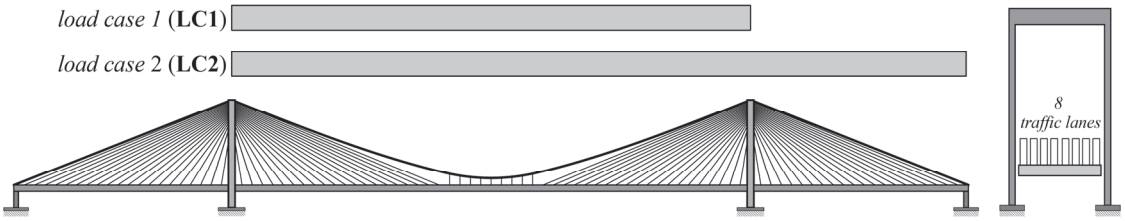

Figure 5: Load cases utilized in the numerical results.

Traffic loads are assumed of 9 kN/m/lane as specified by codes [42]. Furthermore, live loads are arranged on the girder in two different ways: on the center span only (LC1) and on the center span and one side span (LC2) (Fig. 5). It is worth nothing that, live loads are considered located at the center of the structure and thus no torsional effects are expected.

L	1000	m	l	420	m	Δ^G	20	m
c	0.40	-	H	160	m	Δ^P	2	m
μ	0.40	-	f	125	m	L'	20	m
ζ	0.125	-	h^G	3.10	m	$E^{G,P}$	2.1×10^5	MPa
ε_F	0.30	-	b^P	11.24	m	E^C	2.05×10^5	MPa
I_r	50	-	h^P	16.86	m	$S_y^{G,P}$	450	MPa
b^G	33	m	δ^P	0.1124	m	S_y^C	1.6×10^3	MPa
δ^G	0.033	m	p/g^G	0.312	-	$\gamma^{G,P}$	78.5	kN/m^3

Girder cross-section

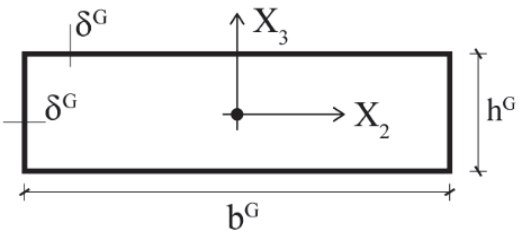

Pylon cross-section

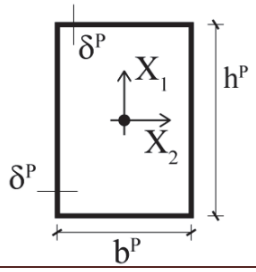

Table 1: Geometric and mechanical properties utilized in the numerical analyses.

Model	Girder and Pylons	Cables
EMB	Elastic	Elastic
CMI	Elastic	Inelastic
BMI	Inelastic	Elastic
FMI	Inelastic	Inelastic

Table 2: Schematic representation of the bridge models.

Investigation on the influence of material nonlinearities

At first, an investigation on the influence of the nonlinear material behavior of structural members on the maximum load carrying capacity of the bridge is developed. To this end, a self-anchored cable-stayed suspension bridge, defined on the basis of the data reported in Tab. 1, is analyzed by using four different types of modeling. The approaches adopted in the analyses are summarized

in Tab. 2. The first model, based on Elastic Material Behavior, namely EMB, considers only the material nonlinearities produced by large displacement effects in the bridge components. Additional models in which a single source of material nonlinearity due to inelastic effects involved in the cables or in both girder and pylons, namely Cable Material Inelastic (CMI) or Beam Material Inelastic (BMI), are analyzed. Finally, a generalized model, which takes into account all geometric and material nonlinearities is also considered, namely Fully Material Inelastic (FMI). For each models, comparisons in terms of load multiplier (λ) as a function of the dimensionless lateral deflection (δ_l / L) at the midpoint of the left side span are presented in Fig. 6 a-b. The results denote that, for low values of load multipliers, all models present the same prediction in the load-displacement curves, since for these load levels an elastic behavior of the bridge is expected. Subsequently, as far as the load level increases, material and geometrical nonlinearities affect the structural behavior, since different evolution laws in terms of maximum load multipliers and load-displacement curves are observed. The analyses show that the maximum carrying capacity of the bridge is quite affected by the material inelastic behavior of structural members. As a matter of fact, load multipliers obtained by EMB model are 93% and 43% larger than that obtained by FMI approach in the case of LC1 and LC2 loading schemes, respectively. Such differences are produced mainly by the material nonlinear behavior of girder and pylons members, since the observed predictions for FMI and BMI models are much lower than the corresponding ones obtained by using other bridge definition, i.e. below 12%. In addition, a lower value of macroscopic ductility of the bridge structure is observed, since the ultimate displacements are much lower than the ones involved in the EMI or CMI scenarios. In particular, for both load cases, the evolution of bridge structure is affected by plastic phenomena which firstly occur at pylon bases, subsequently, at girder side spans and finally at anchor cables. Once that the anchor cables reach the ultimate condition, the structure is not able of bearing further load increments and an abrupt change occurs in the load-displacement curves path. The distribution of the damage parameters involved in girder and cable elements are presented in Fig. 7 a-b, in which the values of state plastic variables, i.e. (α^G, η^G), at the maximum load multiplier are presented. Results denote that for both load cases similar plastic deformation rates between FMI and BMI or EMI and CMI curves are observed. However, FMI and BMI approaches involve lower stresses in the cable system than the ones observed in the analyses developed by using CMI and EMI approaches. Furthermore, the results obtained with the FMI approach predicts that all cables are in the elastic range with the exception of the anchor ones, which exceed the yield stress about 4.2% and 6.7% for LC1 and LC2, respectively. FMI and BMI approaches predict in the girder plastic zones located at the beginning of both side spans or at the left ones only for LC1 or LC2, respectively. Such effects can be also analyzed in terms of girder deformations from the deformed shapes reported in Fig. 8, which show how in the region in which plastic deformations occur relevant displacements are observed.

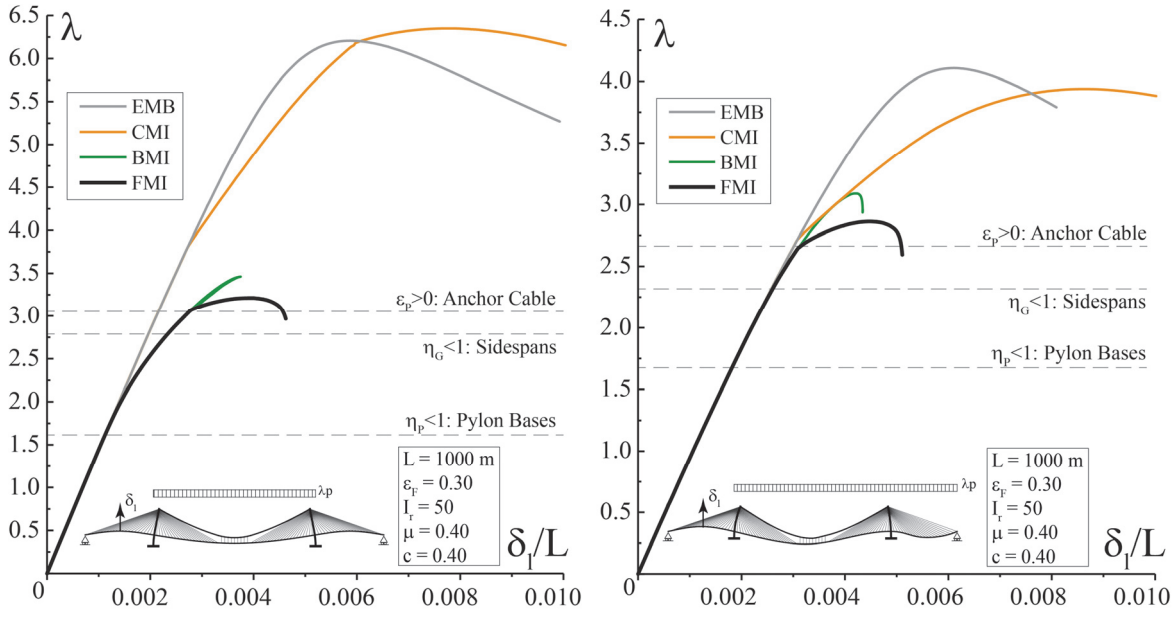

(a) LC1 loading condition. (b) LC2 loading condition.

Figure 6: Load-displacement curve: influence of the bridge formulation.

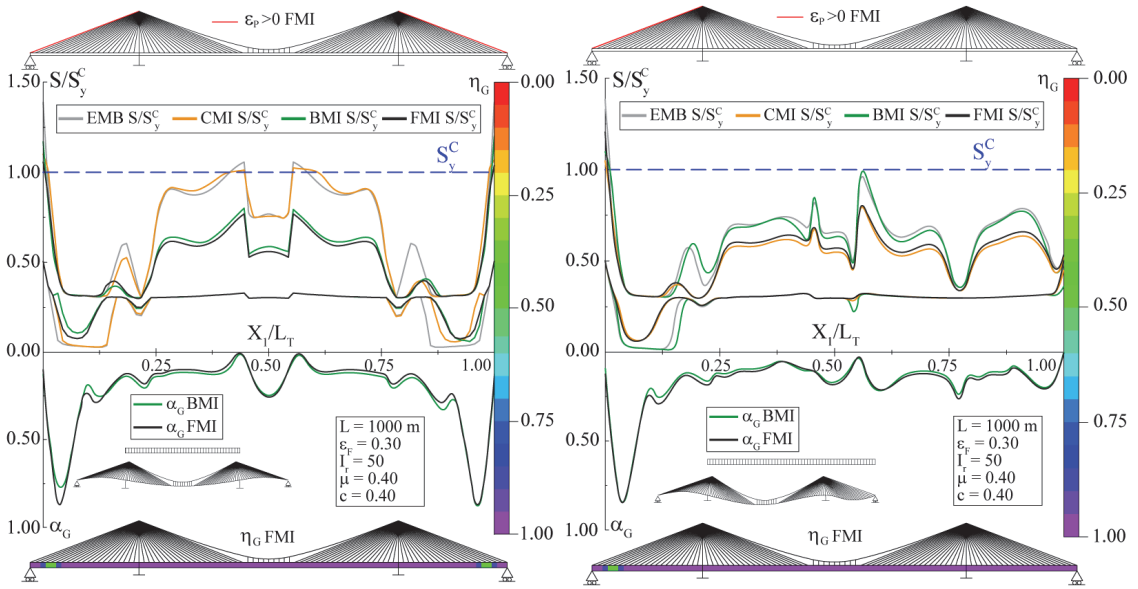

(a) LC1 loading condition (b) LC2 loading condition

Figure 7: Force-state parameter α^G and dimensionless reduction parameter η^G; Maximum cable stresses.

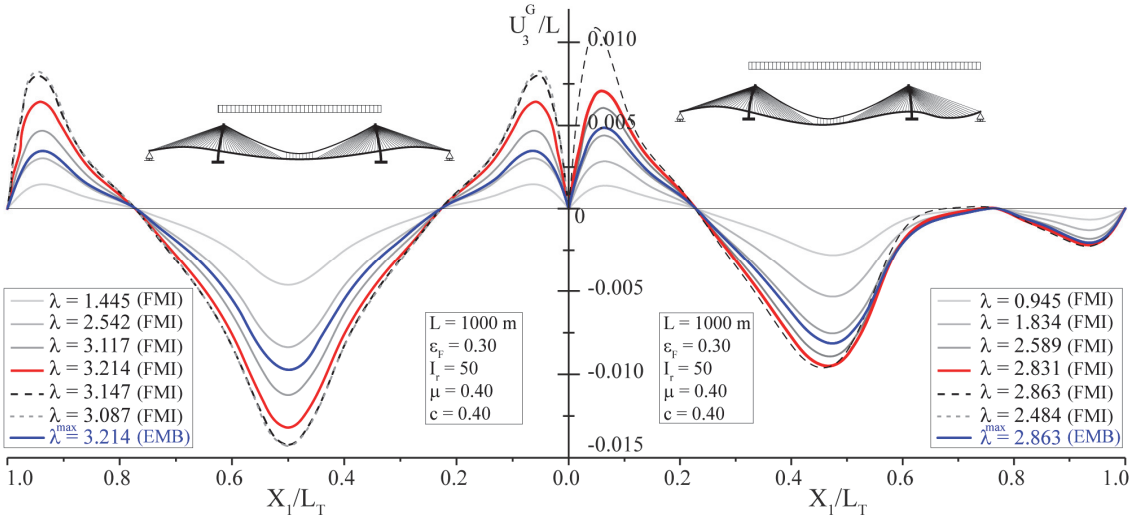

Figure 8: Deformed configurations for different load levels.

Parametric Study

A parametric study is developed in terms of structural characteristics of the bridge components to investigate the variability of the maximum carrying capacity of the bridge scheme. In such analyses, a self-anchored cable-stayed suspension bridge with midspan length (L), height-span ratio (μ) and tower to girder bending stiffness ratio (I_r) equal to 1000 m, 0.4 and 25, respectively, is considered. At first, the influence of the cable-stayed portion (L_{CS}) on the main span of the girder in terms of dimensionless parameter c, with $c = L_{CS}/L$, is investigated. The results, reported in Fig. 9, show the variability of the maximum load multiplier, as a function of dimensionless parameter c, for bending stiffness dimensionless parameters ε_F equal to 0.25, 0.30 and 0.35 and for both LC1 and LC2 loading schemes. The analyses denote that the load-carrying capacity grows for increasing values of the c parameter, leading to maximum load multipliers larger than 6, 10 or 15 times than those obtained in the case of small cable-stayed portions. Such predictions can be explained due to the fact that low values of the dimensionless variable c lead to bridge structures, in which the critical mode producing instability affects the central span, since the cable-stayed system is distributed on a small portion of the

main span. On the other hand, large values of c lead to stiffer bridge structures and larger maximum load multipliers, since the cable-stayed system affects mostly the main span length, giving rise to a notable constraint to the instability vertical deformation modes. The curves obtained in terms of dimensionless parameter ε_F denote how notable improvements to the maximum load multipliers are observed for increasing values of girder stiffness, especially in the range of c between 0.30 and 0.45. Contrarily, as far as the cable-stayed portion is reduced, i.e. for values of c lower than 0.30, the influence of girder stiffness becomes negligible, since a prevailing truss scheme of the bridge is achieved. As a consequence, the same prediction of the maximum load multipliers is observed. Such behavior can be analyzed also numerically by means of the results reported in Tab. 3, in which the variability of the load carrying capacity λ as a function of cable-stayed dimensionless parameter c, relative bending stiffness ε_F and bridge formulation is reported. Additional analyses are developed with the purpose to investigate the variability of the maximum load multiplier in terms of the stay step size along the pylon height. The results are shown in Fig. 10, in which analyses for LC1 and LC2 loading conditions and for several values of the height to span ratio, i.e. $\mu = H / cl = 0.4 - 0.5$, are reported. The parametric study is carried out for bridge schemes in which the cable-stayed portion is based on several arrangements. In particular, four types of cable-stayed configurations are considered: fan, harp and two semi-fan systems with different pylon steps (Δ^P) equal to $L/500$ or $L/200$. Results show that in the case of LC1 loading condition, the prediction of maximum load carrying capacity is practically unaffected from the cable-system geometry, since almost the same prediction is observed for all bridge structures. On the other hand, for the LC2 loading condition a different configuration of the cable-stayed system is able to produce discrepancies in terms of maximum loading factor estimates. However, such behavior can be explained in view of the mutual coupling effects between cable-stayed and suspension system. In particular, for the fan system the transferring of the external loads is mainly dominated by the main cable and the anchor cables and not by the internal elements of the cable-stayed system. On the contrary, in the case of the harp system both suspension and cable-stayed systems contribute to the ultimate carrying capacity of the structure and thus a different prediction is observed. Moreover, for large values of μ the harp scheme provides the best performance in terms of maximum loading factor, since it is able, in view of its cable distribution on the pylon, to constrain the girder deformations.

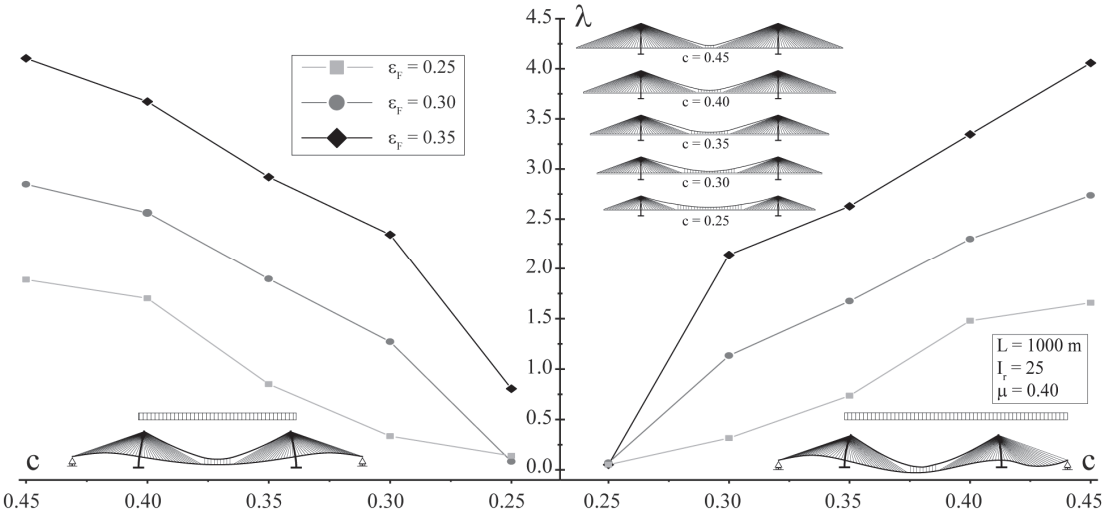

Figure 9: Variability of the length of cable-stayed portion (c), for several values of ε_F parameter

Such phenomena are quite evident from the results reported in Fig. 11, in which the distribution of the stiffness reduction factors η^P and η^G (Fig. 11-a) as well as the evolution of girder and pylon displacements for harp and fan systems (Fig. 11-b) are reported. The results show that in the case of the harp system, the bearing capacity is mostly affected by material nonlinearities since the predicted maximum load multiplier leads to the formation of a plastic hinge located at the base of the left pylon.

c	MODEL	$\varepsilon_F = 0.25$		$\varepsilon_F = 0.30$		$\varepsilon_F = 0.35$	
		LC1	LC2	LC1	LC2	LC1	LC2
0.25	*EMB*	0.14	0.08	0.08	0.07	0.80	0.05
	CMI	0.14	0.08	0.08	0.07	0.80	0.05
	BMI	0.14	0.08	0.08	0.07	0.80	0.05
	FMI	0.14	0.08	0.08	0.07	0.80	0.05
0.30	*EMB*	0.33	0.31	1.29	1.14	2.81	2.40
	CMI	0.33	0.31	1.29	1.14	2.81	2.40
	BMI	0.33	0.31	1.27	1.13	2.34	2.14
	FMI	0.33	0.31	1.27	1.13	2.34	2.14
0.35	*EMB*	0.85	0.74	2.19	1.81	4.52	3.51
	CMI	0.85	0.73	2.19	1.81	4.19	3.18
	BMI	0.85	0.73	1.90	1.67	3.03	2.72
	FMI	0.85	0.73	1.90	1.67	2.92	2.63
0.40	*EMB*	2.00	1.63	4.28	3.24	8.44	5.84
	CMI	1.84	1.53	4.10	2.89	9.07	5.49
	BMI	1.72	1.49	2.82	2.51	4.06	3.70
	FMI	1.70	1.48	2.56	2.30	3.67	3.35
0.45	*EMB*	3.36	2.56	7.40	5.13	14.65	9.23
	CMI	3.61	2.46	8.79	5.25	16.10	9.89
	BMI	2.08	1.91	3.21	3.08	4.69	4.53
	FMI	1.89	1.66	2.85	2.74	4.11	4.06

Table 3: Load multiplier as a function of c and ε_F parameters for $I_r = 25$ and $\mu = 0.40$.

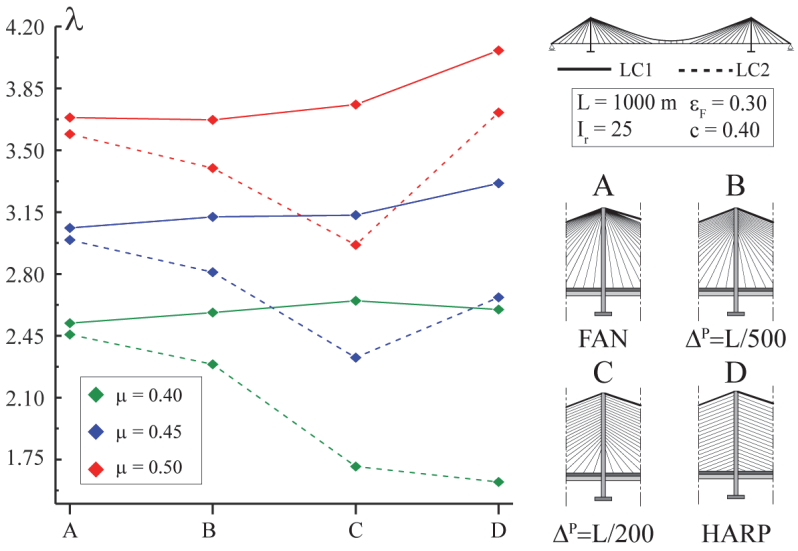

Figure 10: Variability of the cable-stayed system configuration.

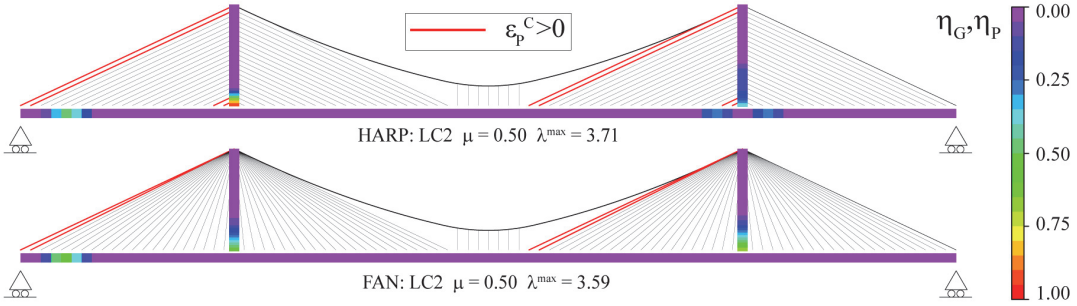

(a) Girder and pylons dimensionless reduction parameters

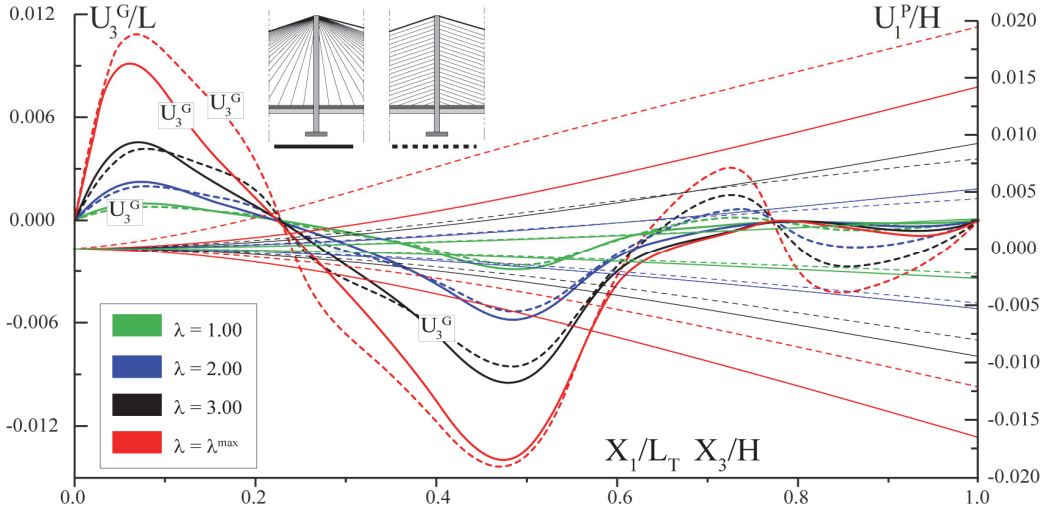

(b) Girder and pylons deformed configurations for different load levels

Figure 11: Comparisons between fan and harp cable-stayed configuration for LC2.

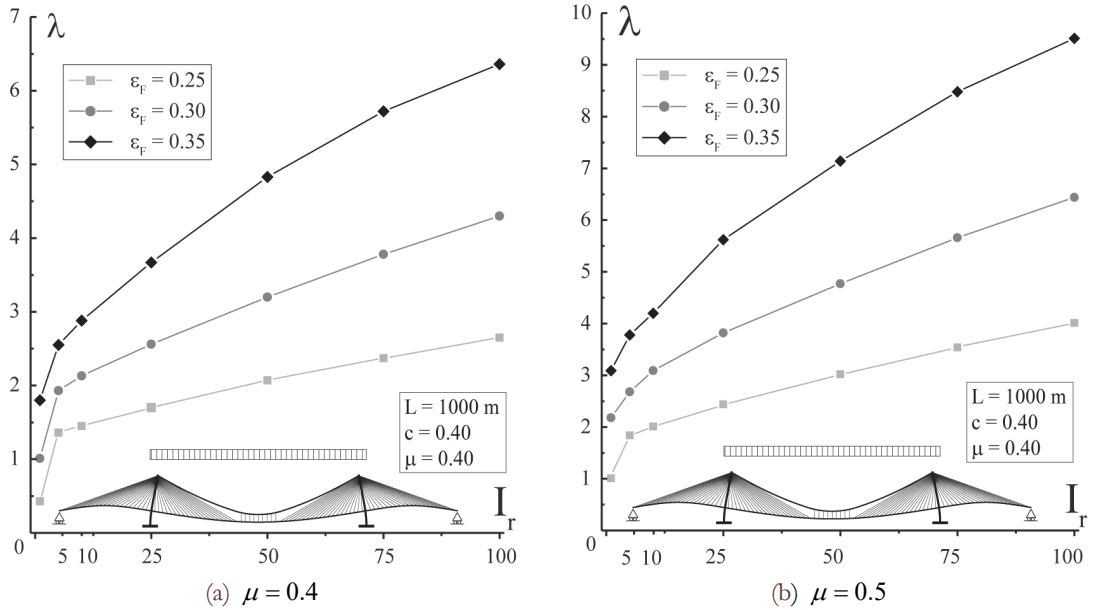

(a) $\mu = 0.4$ (b) $\mu = 0.5$

Figure 12: Variability of tower to girder bending stiffness ratio I_r, for several values of relative girder bending stiffness ε_F

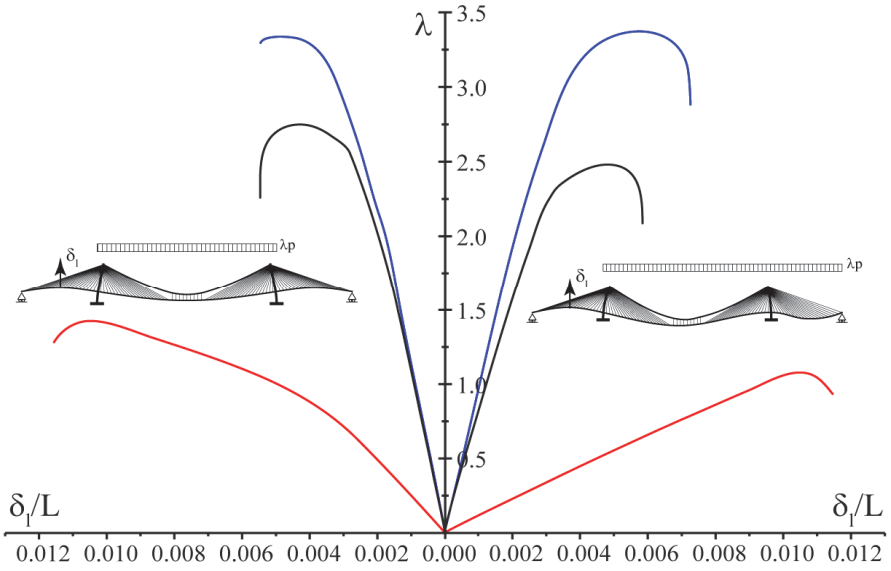

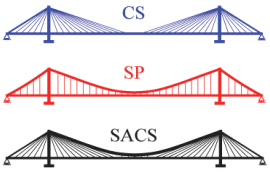

CS	SACS	SP
H/L = 0.50	H/L = 0.16	H/L = 0.115
-	f/L = 0.125	f/L = 0.10
-	c = 0.40	-
L = 1000 m		
l/L = 0.42		
b^G/L= 0.033 h^G/b^G= 0.105 b^G/δ^G= 1000		
h^G/h^P = 0.245 h^P/b^P = 1.50 b^P/δ^P = 100		

Figure 13: Comparisons between bridges typologies in terms of load-displacement curve.

Such collapse mechanism was not observed in the fan configuration, in which both girder and pylons are affected by larger displacements. Further results are developed to investigate the influence of girder and pylon properties on the load carrying capacity of the bridge. In particular, in Fig. 12 a-b, maximum allowable load multipliers versus bending stiffness ratio I_r, with $I_r = I_2^P / I_2^G$, for several values of the relative girder bending stiffness and height-span ratio, i.e. $\varepsilon_F = [0.25, 0.30, 0.35]$ and $\mu = [0.4 - 0.5]$, respectively, are reported. For sake of brevity, only results related to LC1 loading condition are presented. The load multiplier distribution denotes a tendency to increase with respect to the parameters I_r, ε_F and μ. It is worth nothing that the sudden fall of load multipliers for values of I_r lower than 5 can be explained in view of local buckling phenomena occurring in pylon members. For increasing values of I_r, the failure condition is reached in the girder and thus the observed loading multipliers are much larger.

Finally, results are proposed to evaluate the behavior of self-anchored cable-stayed suspension bridges in comparison to bridge structures based on pure cable-stayed and self-anchored suspension systems. The main purpose of the present analysis is to investigate the influence of the cable system configuration on the nonlinear behavior and the prediction of the maximum carrying capacity of the bridge structure. Since each bridge scheme is characterized by specific height to span ratios, such quantities are assumed to be different in the analysis. However, equal main span length, girder and pylon characteristics are assumed for all bridge schemes considered in the present analyses. The maximum load carrying capacity is predicted by mean of the proposed FMI model. The results are presented in Fig. 13, in which the evolution of load multipliers λ as a function of the dimensionless lateral deflection (δ_l / L) at the midpoint of the left side span is analyzed. Moreover, in Fig. 14 a-b girder deformed shapes at the maximum value of load multiplier for LC1 and LC2 loading schemes, respectively, are reported. The results show that the cable-stayed bridge scheme presents the largest values of the load multipliers than those observed for the remaining cable supported systems. Moreover, with respect to the cable-stayed system, the pure suspension or the self-anchored schemes present a lower load carrying capacity with percentage reduction factors equal to 58% and 18% or 68% and 26% for LC1 or LC2 loading conditions, respectively. The pure cable-stayed and hybrid cable-stayed suspension systems have similar girder deformations at failure for both load cases (Fig. 14 a-b) and they are affected by the largest value of vertical displacements in the region close to the midspan girder cross-section of bridges. On the other hand, the suspension scheme has its maximum vertical displacement at the midpoint of side spans. Such mechanisms can be explained by the characteristics of the suspension system of the hybrid bridge scheme, in relationship to the improved stiffness behavior of the main cable with respect to midspan vertical displacements. Such aspect denotes that the cable-stayed portion of the hybrid configuration highly affects the structural behavior of the entire system, providing improvements to the self-anchored bridge typology. This suggests that the self-anchored hybrid configuration can be a good alternative to the pure cable-stayed system for midspan length close to 1000 m, which is currently the limit operating range of actual cable-stayed bridges.

In order to verify the effectiveness of the self-anchored cable-stayed suspension system in the framework of long span bridges, additional results are presented for a bridge scheme whose main span length is equal to 1500 m.

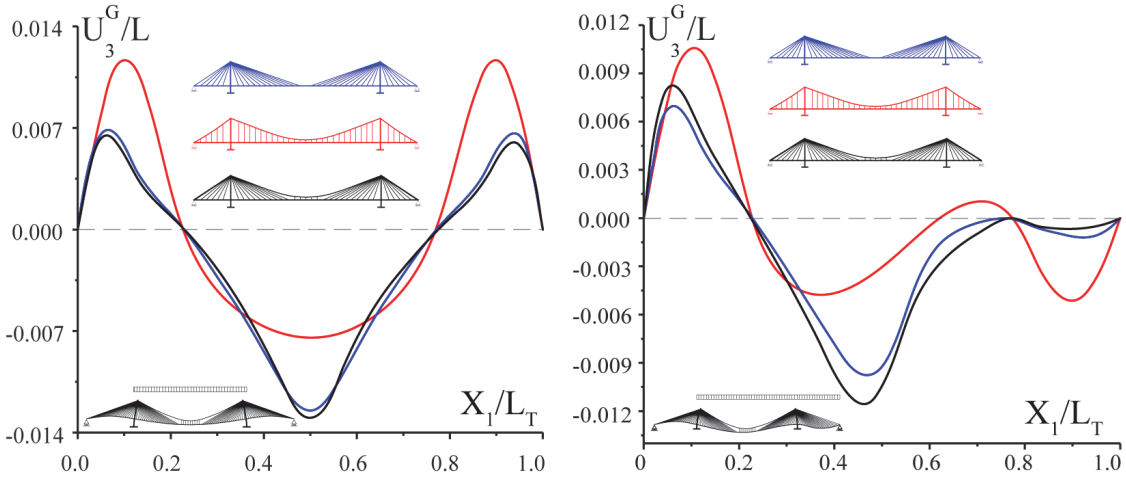

(a) LC1 loading condition (b) LC2 loading condition

Figure 14: Comparisons between bridges typologies in terms of dimensionless girder vertical displacements (U_G^3/L) at maximum values of load parameter λ

In such analyses, the comparisons are restricted to the pure self-anchored suspension and the hybrid cable stayed suspension bridges. The results, presented in Fig. 15, show that the self-anchored hybrid system has a load carrying capacity almost two times larger than that related to the pure suspension one. Such results, together with previous comparisons, point out the enhanced properties of the self-anchored hybrid configuration, which ensures notable structural performances for both medium and long main span lengths.

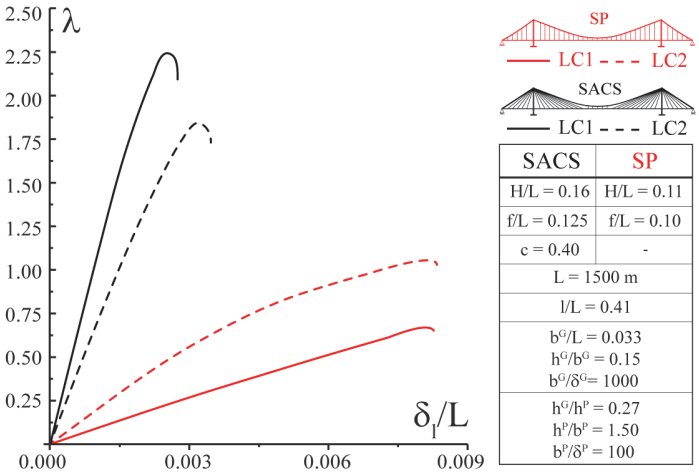

SACS	SP
H/L = 0.16	H/L = 0.11
f/L = 0.125	f/L = 0.10
c = 0.40	-
L = 1500 m	
l/L = 0.41	
$b^G/L = 0.033$ $h^G/b^G = 0.15$ $b^G/\delta^G = 1000$	
$h^G/h^P = 0.27$ $h^P/b^P = 1.50$ $b^P/\delta^P = 100$	

Figure 15: Loading curve of midspan vertical displacement (δ_1/L): comparisons between hybrid and suspension bridge scheme.

CONCLUSIONS

The main aim of the present paper is to analyze the influence of the nonlinear material behavior and structural characteristics of self-anchored cable-stayed suspension bridges on the maximum loading carrying capacity. To this end, a parametric study is developed in terms of bridge characteristics, involving geometric, material and mechanical properties of the bridge constituents. Moreover, in order to verify the effectiveness of the self-anchored

bridge typologies, comparisons with existing schemes based on pure cable-stayed and suspension systems are presented. From the results, the following conclusions can be drawn:

- the inelastic material behavior affects significantly the maximum load carrying capacity of the bridge structure. Models which exclude the inelastic behavior of structural members may lead to a generalized overestimation of the loading bearing capacity of the structure.
- The bearing capacity of the bridge structure increases with the length of cable-stayed portion and the inelastic material behavior affects the maximum carrying capacity especially in the case of cable-stayed dominated bridge schemes.
- Large values of girder and pylon bending stiffnesses lead to considerable benefits in terms of load bearing capacity, avoiding local instabilities due to buckling effects.
- The cable-stayed portion, based on a fan, semi-fan or harp configurations, strongly affects the load bearing capacity of the structure. The fan system involves the best performances especially with reference to low values of the height-span ratio.
- From the parametric studies developed in terms of material and geometric characteristics of both girder and pylons, suspension system configuration, it transpires that self-anchored cable-stayed suspension bridges may be considered as an enhanced opportunity to overcome long spans with respect to conventional bridge schemes based on pure cable-stayed or suspension systems.

REFERENCES

[1] Gimsing, N.J., Georgakis, C.T., Cable supported bridges. Concept and design. Third ed.: John Wiley & Sons, Ltd. (2012).
[2] Troitsky, M.S., Cable-stayed bridges. Theory and design. Second ed: BSP Professional Booka, Oxford, (1988).
[3] Oliveira, D.V., Lourenço, P.B., Lemos, C., Geometric issues and ultimate load capacity of masonry arch bridges from the northwest Iberian Peninsula. Engineering Structures, 32 (2010) 3955-3965. DOI: 10.1016/j.engstruct.2010.09.006.
[4] Fasoulakis, Z.C., Avraam, T.P., Raftoyiannis, I.G., Dynamic buckling of partially-sway frames with varying stiffness using catastrophe theory. International Journal of Non-Linear Mechanics, 71 (2015) 116-126. DOI: 10.1016/j.ijnonlinmec.2014.10.002.
[5] Tang, M.-C., Buckling of cable-stayed girder bridges. ASCE J Struct Div, 102 (1976) 1675-1684.
[6] Nagai, M., Asano, K., Watanabe, K., Applicability of the Ef method and design method for evaluating the load-carrying capacity of girders in cable-stayed bridges. Journal of Structural Engineering, 41 (1995) 221-228.
[7] Xi, Y., Kuang, J.S., Ultimate load capacity of cable-stayed bridges. Journal of Bridge Engineering, 4 (1999) 14-21.
[8] Nakai, H., et al., Elasto-plastic and finite displacement analysis of cable-stayed bridges. Memoirs of the Faculty of Engineering, Osaka City University, 26 (1985) 251-271.
[9] Kim, S.E., Park, M.H., Choi, S.H., Direct design of three-dimensional frames using practical adavanced analysis. Engineering Structures, 26 (2001) 1491-1502.
[10] Iwasaki, H., Nogami, K., Nagai, M., Precision of EF method for evaluating load-carrying capacity of long-span cable-stayed bridges and its ultimate strength check, in Cable-Supported Bridges - Challenging Technical Limits. International Association for Bridge and Structural Engineering, Seoul, (2001) 17-24.
[11] Tomblin, J., Barbero, E., Local buckling experiments on FRP columns. Thin-Walled Structures, 18 (1994) 97-116.
[12] Yoo, H., Choi, D.H., New method of inelastic buckling analysis for steel frames. Journal of Constructional Steel Research, 64 (2008) 1152-1164. DOI: 10.1016/j.jcsr.2008.01.024.
[13] Yoo, H., Na, H.S., Choi, D.H., Approximate method for estimation of collapse loads of steel cable-stayed bridges. Journal of Constructional Steel Research, 72 (2012) 143-154. DOI: 10.1016/j.jcsr.2011.12.003
[14] Seif, S.P., Dilger, W.H., Nonlinear analysis and collapse load of P/C cable-stayed bridges. Journal of structural engineering New York, N.Y., 116 (1990) 829-849.
[15] Xie, X., Nagai, M., Yamaguchi, H., Elasto-plastic finite displacement analysis of loan-span cable-stayed bridges including inelastic behavior of cables. Journal of Structural Engineering, JSCE, 44 (1998) 229-236.
[16] Ren, W.X., Ultimate behavior of long-span cable-stayed bridges. Journal of Bridge Engineering, 4 (1999) 30-37.
[17] Choi, D.H., et al., Ultimate behavior and ultimate load capacity of steel cable-stayed bridges. Structural Engineering and Mechanics, 27 (2007) 477-499.
[18] Barbié, L., Ramière, I., Lebon, F., An automatic multilevel refinement technique based on nested local meshes for nonlinear mechanics. Computers and Structures, 14 (2014) 14-25. DOI: 10.1016/j.compstruc.2014.10.008.

[19] Orbison, J., Nonlinear static analysis of three-dimensional steel frames. Cornell University, Ithaca, New York, (1982).
[20] Liew, J., Tang, L., Nonlinear refined plastic hinge analysis of space frame structure. National university of Singapore, Singapore (1988).
[21] Kim, S.E., Kim, M.K., Chen, W.F., Improved refined plastic hinge analysis accounting for strain reversal. Engineering Structures, 22 (2000) 15-25. DOI: 10.1016/S0141-0296(98)00079-0.
[22] Thai, H.T., Kim, S.E., Second-order inelastic dynamic analysis of steel frames using fiber hinge method. Journal of Constructional Steel Research, 67 (2011) 1485-1494. DOI: 10.1016/j.jcsr.2011.03.022.
[23] Thai, H.T., Kim, S.E., Second-order inelastic analysis of cable-stayed bridges. Finite Elements in Analysis and Design, 53 (2012) 48-55. DOI: 10.1016/j.finel.2011.07.002
[24] Nagai, M., Iwasaki, H., Nogami, K.. Effect of inelastic behavior of cables on ultimate behavior and strength of a 600-m steel cable-stayed bridge. in Second MIT conference on Computational Fluid and Solid Mechanics. (2003).
[25] Zhang, Z., et al., Limit span of self-anchored cable-stayed suspension cooperation system bridge based on strength. Frontiers of Architecture and Civil Engineering in China, 3 (2009) 286-291.
[26] Zhang, Z., et al., Study of limit span of self-anchored cable-stayed suspension cooperation system bridge based on strength. Dalian Ligong Daxue Xuebao/Journal of Dalian University of Technology, 48 (2008) 387-391.
[27] Hui-Li, W., et al., Geometric nonlinear analysis of self-anchored cable-stayed suspension bridges. The Scientific World Journal, (2013). DOI: 10.1155/2013/734387.
[28] Wang, H.L., et al., The Basic differential equations of self-anchored cable-stayed suspension bridge. Mathematical Problems in Engineering, (2010). DOI: 10.1155/2010/805195.
[29] Lonetti, P., Pascuzzo, A., Design analysis of the optimum configuration of self-anchored cable-stayed suspension bridges. Structural Engineering and Mechanics, 51 (2014) 847-866. DOI: 10.12989/sem.2014.51.5.847.
[30] Bruno, D., Greco, F., Lonetti, P., Dynamic impact analysis of long span cable-stayed bridges under moving loads. Engineering Structures, 30 (2008) 1160-1177. DOI: 10.1016/j.engstruct.2007.07.001.
[31] Bruno, D., Lonetti, P., Pascuzzo, A., An optimization model for the design of network arch bridges. Computers & Structures, 170 (2016) 13-25. DOI: 10.1016/j.compstruc.2016.03.011.
[32] Lonetti, P., Pascuzzo, A., Davanzo, A., Dynamic Behavior of Tied-Arch Bridges under the Action of Moving Loads. Mathematical Problems in Engineering, (2016). DOI: 10.1155/2016/2749720.
[33] Kim, S.E., Choi, S.H., Practical second-order inelastic analysis for three-dimensional steel frames subjected to distributed load. Thin-Walled Structures, 43 (2005) 135-160. DOI: 10.1016/j.tws.2004.09.001.
[34] Chan, S.L., Chui, P.P.T., Non-linear static analysis allowing for plastic hinges and semi-rigid joints, in: Non-Linear Static and Cyclic Analysis of Steel Frames with Semi-Rigid Connections, S.L.C.P.T. Chui, Elsevier Science Ltd, Oxford, (2009) 123-194.
[35] Greco, F., Lonetti P., Pascuzzo, A., Dynamic analysis of cable-stayed bridges affected by accidental failure mechanisms under moving loads. Mathematical Problems in Engineering, (2013). DOI: 10.1155/2013/302706.
[36] Lonetti, P., Pascuzzo, A., Vulnerability and failure analysis of hybrid cable-stayed suspension bridges subjected to damage mechanisms. Engineering Failure Analysis, 45 (2014) 470-495. DOI: 10.1016/j.engfailanal.2014.07.002.
[37] Bruno, D., Greco, F., Lonetti, P., A parametric study on the dynamic behavior of combined cable-stayed and suspension bridges under moving loads. International Journal of Computational Methods in Engineering Science and Mechanics, 10 (2009), 243-258. DOI: 10.1080/15502280902939452.
[38] Papadopoulos, P., Lu, J., A general framework for the numerical solution of problems in finite elasto-plasticity. Computer Methods in Applied Mechanics and Engineering, 159 (1998) 1-18. DOI: 10.1016/S0045-7825(98)80101-1.
[39] Papadopoulos, P., Lu, J., On the formulation and numerical solution of problems in anisotropic finite plasticity. Computer Methods in Applied Mechanics and Engineering, 190 (2001) 4889-4910. DOI: 10.1016/S0045-7825(00)00355-8.
[40] COMSOL, Reference manual. (2012).
[41] Lonetti, P., Pascuzzo, A., Optimum design analysis of hybrid cable-stayed suspension bridges. Advances in Engineering Software, 73 (2014) 53-66. DOI: 10.1016/j.advengsoft.2014.03.004.
[42] Highway, A.A.o.S. and T. Officials, AASHTO LRFD bridge design specifications: customary U.S. Units. American Association of State Highway and Transportation Officials, (2007).